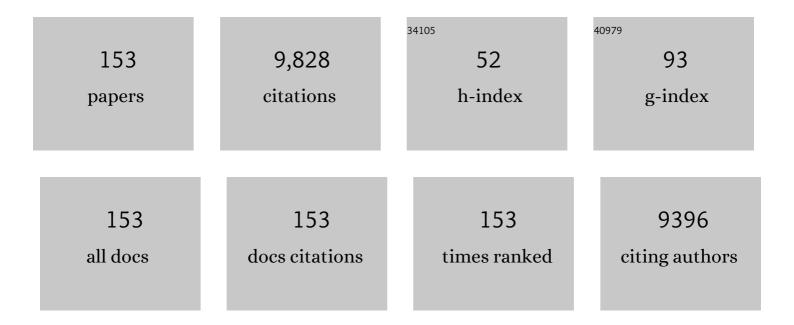
## Yuanyuan Wang

List of Publications by Year in descending order

Source: https://exaly.com/author-pdf/2741271/publications.pdf Version: 2024-02-01



#	Article	IF	CITATIONS
1	Oxygen Vacancy Induced Band-Gap Narrowing and Enhanced Visible Light Photocatalytic Activity of ZnO. ACS Applied Materials & Interfaces, 2012, 4, 4024-4030.	8.0	1,269
2	In situ ion exchange synthesis of the novel Ag/AgBr/BiOBr hybrid with highly efficient decontamination of pollutants. Chemical Communications, 2011, 47, 7054.	4.1	433
3	Composite of CH <sub>3</sub> NH <sub>3</sub> PbI <sub>3</sub> with Reduced Graphene Oxide as a Highly Efficient and Stable Visibleâ€Light Photocatalyst for Hydrogen Evolution in Aqueous HI Solution. Advanced Materials, 2018, 30, 1704342.	21.0	302
4	Hydrogenated titania: synergy of surface modification and morphology improvement for enhanced photocatalytic activity. Chemical Communications, 2012, 48, 5733.	4.1	285
5	Honeycomb Carbon Nanofibers: A Superhydrophilic O <sub>2</sub> â€Entrapping Electrocatalyst Enables Ultrahigh Mass Activity for the Twoâ€Electron Oxygen Reduction Reaction. Angewandte Chemie - International Edition, 2021, 60, 10583-10587.	13.8	219
6	Cu <sub>2</sub> 0 Nanoparticles with Both {100} and {111} Facets for Enhancing the Selectivity and Activity of CO <sub>2</sub> Electroreduction to Ethylene. Advanced Science, 2020, 7, 1902820.	11.2	196
7	Highâ€Performance Electrochemical NO Reduction into NH <sub>3</sub> by MoS <sub>2</sub> Nanosheet. Angewandte Chemie - International Edition, 2021, 60, 25263-25268.	13.8	180
8	Ambient Ammonia Synthesis via Electrochemical Reduction of Nitrate Enabled by NiCo <sub>2</sub> O <sub>4</sub> Nanowire Array. Small, 2022, 18, e2106961.	10.0	171
9	Synthesis of synergetic phosphorus and cyano groups ( C N) modified g-C3N4 for enhanced photocatalytic H2 production and CO2 reduction under visible light irradiation. Applied Catalysis B: Environmental, 2018, 232, 521-530.	20.2	162
10	Metallic zinc- assisted synthesis of Ti <sup>3+</sup> self-doped TiO <sub>2</sub> with tunable phase composition and visible-light photocatalytic activity. Chemical Communications, 2013, 49, 868-870.	4.1	159
11	Enhancing the Photocatalytic Hydrogen Evolution Activity of Mixed-Halide Perovskite CH <sub>3</sub> NH <sub>3</sub> PbBr <sub>3–<i>x</i></sub> I <sub><i>x</i></sub> Achieved by Bandgap Funneling of Charge Carriers. ACS Catalysis, 2018, 8, 10349-10357.	11.2	159
12	Doping strategy to promote the charge separation in BiVO4 photoanodes. Applied Catalysis B: Environmental, 2017, 211, 258-265.	20.2	156
13	Preparation of a morph-genetic CaO-based sorbent using paper fibre as a biotemplate for enhanced CO2 capture. Chemical Engineering Journal, 2019, 361, 235-244.	12.7	139
14	Adsorption of gaseous ethylene via induced polarization on plasmonic photocatalyst Ag/AgCl/TiO2 and subsequent photodegradation. Applied Catalysis B: Environmental, 2018, 220, 356-361.	20.2	134
15	In-situ phosphating to synthesize Ni2P decorated NiO/g-C3N4 p-n junction for enhanced photocatalytic hydrogen production. Chemical Engineering Journal, 2019, 378, 122161.	12.7	133
16	WS <sub>2</sub> /Graphitic Carbon Nitride Heterojunction Nanosheets Decorated with CdS Quantum Dots for Photocatalytic Hydrogen Production. ChemSusChem, 2018, 11, 1187-1197.	6.8	129
17	Fabrication of carbon bridged g-C3N4 through supramolecular self-assembly for enhanced photocatalytic hydrogen evolution. Applied Catalysis B: Environmental, 2018, 229, 114-120.	20.2	128
18	Perovskite photocatalyst CsPbBr3-xIx with a bandgap funnel structure for H2 evolution under visible light. Applied Catalysis B: Environmental, 2019, 245, 522-527.	20.2	127

#	Article	IF	CITATIONS
19	Light-Promoted CO <sub>2</sub> Conversion from Epoxides to Cyclic Carbonates at Ambient Conditions over a Bi-Based Metal–Organic Framework. ACS Catalysis, 2021, 11, 1988-1994.	11.2	117
20	High-efficient electrocatalytic overall water splitting over vanadium doped hexagonal Ni0.2Mo0.8N. Applied Catalysis B: Environmental, 2020, 263, 118330.	20.2	111
21	TiO2/Ti3C2 as an efficient photocatalyst for selective oxidation of benzyl alcohol to benzaldehyde. Applied Catalysis B: Environmental, 2021, 286, 119885.	20.2	111
22	Design and synthesis of porous M-ZnO/CeO2 microspheres as efficient plasmonic photocatalysts for nonpolar gaseous molecules oxidation: Insight into the role of oxygen vacancy defects and M=Ag, Au nanoparticles. Applied Catalysis B: Environmental, 2020, 260, 118151.	20.2	110
23	2D/2D heterostructure of ultrathin BiVO4/Ti3C2 nanosheets for photocatalytic overall Water splitting. Applied Catalysis B: Environmental, 2021, 285, 119855.	20.2	109
24	Leadâ€Free Halide Perovskite Cs <sub>3</sub> Bi <sub>2</sub> <i><sub>x</sub></i> Sb <sub>2–2</sub> <i><sub>x</sub></i> ( <i>x</i> <b>â‰^</b> 0.3) Possessing the Photocatalytic Activity for Hydrogen Evolution Comparable to that of (CH <sub>3</sub> NH <sub>3</sub> )Pbl <sub>3</sub> . Advanced Materials, 2020, 32, e2001344.	21.0	107
25	Efficient photocatalytic H2 production via rational design of synergistic spatially-separated dual cocatalysts modified Mn0.5Cd0.5S photocatalyst under visible light irradiation. Chemical Engineering Journal, 2018, 337, 480-487.	12.7	102
26	Electrocatalytic hydrogen peroxide production in acidic media enabled by NiS <sub>2</sub> nanosheets. Journal of Materials Chemistry A, 2021, 9, 6117-6122.	10.3	102
27	Multiple carrier-transfer pathways in a flower-like In <sub>2</sub> S <sub>3</sub> /CdIn <sub>2</sub> S <sub>4</sub> /In <sub>2</sub> O <sub>3</sub> ternary heterostructure for enhanced photocatalytic hydrogen production. Nanoscale, 2018, 10, 7860-7870.	5.6	98
28	An organometal halide perovskite supported Pt single-atom photocatalyst for H <sub>2</sub> evolution. Energy and Environmental Science, 2022, 15, 1271-1281.	30.8	97
29	Electrocatalytic nitrogen reduction on the transition-metal dimer anchored N-doped graphene: performance prediction and synergetic effect. Physical Chemistry Chemical Physics, 2021, 23, 4018-4029.	2.8	90
30	Sulfuration of NiV-layered double hydroxide towards novel supercapacitor electrode with enhanced performance. Chemical Engineering Journal, 2018, 351, 119-126.	12.7	89
31	Synthesis of a WO <sub>3</sub> photocatalyst with high photocatalytic activity and stability using synergetic internal Fe <sup>3+</sup> doping and superficial Pt loading for ethylene degradation under visible-light irradiation. Catalysis Science and Technology, 2019, 9, 652-658.	4.1	86
32	Boosting the electrocatalytic HER performance of Ni3N-V2O3 via the interface coupling effect. Applied Catalysis B: Environmental, 2021, 283, 119590.	20.2	84
33	Selective photocatalytic conversion of alcohol to aldehydes by singlet oxygen over Bi-based metal-organic frameworks under UV–vis light irradiation. Applied Catalysis B: Environmental, 2019, 254, 463-470.	20.2	83
34	Photocatalytic hydrogen evolution on P-type tetragonal zircon BiVO4. Applied Catalysis B: Environmental, 2019, 251, 94-101.	20.2	82
35	Photocatalytic Selective Oxidation of HMF Coupled with H <sub>2</sub> Evolution on Flexible Ultrathin g-C <sub>3</sub> N <sub>4</sub> Nanosheets with Enhanced N–H Interaction. ACS Catalysis, 2022, 12, 1919-1929.	11.2	82
36	Anisotropic Photoelectrochemical (PEC) Performances of ZnO Single-Crystalline Photoanode: Effect of Internal Electrostatic Fields on the Separation of Photogenerated Charge Carriers during PEC Water Splitting. Chemistry of Materials, 2016, 28, 6613-6620.	6.7	81

#	Article	IF	CITATIONS
37	Co3(hexaiminotriphenylene)2: A conductive two-dimensional π–d conjugated metal–organic framework for highly efficient oxygen evolution reaction. Applied Catalysis B: Environmental, 2020, 278, 119295.	20.2	80
38	Conductive Two-Dimensional Magnesium Metal–Organic Frameworks for High-Efficiency O <sub>2</sub> Electroreduction to H <sub>2</sub> O <sub>2</sub> . ACS Catalysis, 2022, 12, 6092-6099.	11.2	78
39	Enhancing electrocatalytic N2-to-NH3 fixation by suppressing hydrogen evolution with alkylthiols modified Fe3P nanoarrays. Nano Research, 2022, 15, 1039-1046.	10.4	74
40	Highly efficient electrocatalytic hydrogen evolution coupled with upcycling of microplastics in seawater enabled via Ni3N/W5N4 janus nanostructures. Applied Catalysis B: Environmental, 2022, 307, 121198.	20.2	72
41	Thermochemical energy storage performance of Al2O3/CeO2 co-doped CaO-based material under high carbonation pressure. Applied Energy, 2020, 263, 114650.	10.1	70
42	Enabling multifunctional electrocatalysts by modifying the basal plane of unifunctional 1T′-MoS <sub>2</sub> with anchored transition metal single atoms. Nanoscale, 2021, 13, 13390-13400.	5.6	69
43	Enhanced Electrochemical H <sub>2</sub> O <sub>2</sub> Production via Two-Electron Oxygen Reduction Enabled by Surface-Derived Amorphous Oxygen-Deficient TiO <sub>2–<i>x</i></sub> . ACS Applied Materials & Interfaces, 2021, 13, 33182-33187.	8.0	67
44	Noble-metal-free Fe2P–Co2P co-catalyst boosting visible-light-driven photocatalytic hydrogen production over graphitic carbon nitride: The synergistic effects between the metal phosphides. International Journal of Hydrogen Energy, 2019, 44, 4133-4142.	7.1	66
45	Accelerated electrocatalytic hydrogen evolution on non-noble metal containing trinickel nitride by introduction of vanadium nitride. Journal of Materials Chemistry A, 2019, 7, 5513-5521.	10.3	65
46	CeO2-modified CaO/Ca12Al14O33 bi-functional material for CO2 capture and H2 production in sorption-enhanced steam gasification of biomass. Energy, 2020, 192, 116664.	8.8	64
47	Fabrication and CO2 capture performance of magnesia-stabilized carbide slag by by-product of biodiesel during calcium looping process. Applied Energy, 2016, 168, 85-95.	10.1	63
48	DFT study of CO2 adsorption across a CaO/Ca12Al14O33 sorbent in the presence of H2O under calcium looping conditions. Chemical Engineering Journal, 2019, 370, 10-18.	12.7	63
49	Synthesis of MoS2/Ni3S2 heterostructure for efficient electrocatalytic hydrogen evolution reaction through optimizing the sulfur sources selection. Applied Surface Science, 2018, 459, 422-429.	6.1	60
50	Carbon nanosheet facilitated charge separation and transfer between molybdenum carbide and graphitic carbon nitride toward efficient photocatalytic H2 production. Applied Surface Science, 2019, 473, 91-101.	6.1	59
51	CaO/Ca(OH)2 thermochemical heat storage of carbide slag from calcium looping cycles for CO2 capture. Energy Conversion and Management, 2018, 174, 8-19.	9.2	57
52	Enhancing the Photoelectrochemical Water Oxidation Reaction of BiVO <sub>4</sub> Photoanode by Employing Carbon Spheres as Electron Reservoirs. ACS Catalysis, 2020, 10, 13031-13039.	11.2	57
53	Theoretical insights into the electroreduction of nitrate to ammonia on graphene-based single-atom catalysts. Nanoscale, 2022, 14, 10862-10872.	5.6	57
54	Co <sub>3</sub> O <sub>4</sub> nanobelt arrays assembled with ultrathin nanosheets as highly efficient and stable electrocatalysts for the chlorine evolution reaction. Journal of Materials Chemistry A, 2018, 6, 12718-12723.	10.3	55

Yuanyuan Wang

#	Article	IF	CITATIONS
55	Effect of the intra- and inter-triazine N-vacancies on the photocatalytic hydrogen evolution of graphitic carbon nitride. Chemical Engineering Journal, 2019, 369, 263-271.	12.7	55
56	Two-dimensional π–d conjugated metal–organic framework Fe3(hexaiminotriphenylene)2 as a photo-Fenton like catalyst for highly efficient degradation of antibiotics. Applied Catalysis B: Environmental, 2021, 290, 120029.	20.2	55
57	Electrochemical two-electron O <sub>2</sub> reduction reaction toward H <sub>2</sub> O <sub>2</sub> production: using cobalt porphyrin decorated carbon nanotubes as a nanohybrid catalyst. Journal of Materials Chemistry A, 2021, 9, 26019-26027.	10.3	55
58	Performance of Li4SiO4 Material for CO2 Capture: A Review. International Journal of Molecular Sciences, 2019, 20, 928.	4.1	54
59	Efficient near-infrared photocatalysts based on NaYF4:Yb3+,Tm3+@NaYF4:Yb3+,Nd3+@TiO2 core@shell nanoparticles. Chemical Engineering Journal, 2019, 361, 1089-1097.	12.7	53
60	Stress-induced BiVO4 photoanode for enhanced photoelectrochemical performance. Applied Catalysis B: Environmental, 2022, 304, 121012.	20.2	52
61	Coupling denitrification and ammonia synthesis <i>via</i> selective electrochemical reduction of nitric oxide over Fe <sub>2</sub> O <sub>3</sub> nanorods. Journal of Materials Chemistry A, 2022, 10, 6454-6462.	10.3	52
62	Oxygenâ€Vacancyâ€Enhanced Singlet Oxygen Production for Selective Photocatalytic Oxidation. ChemSusChem, 2020, 13, 3488-3494.	6.8	51
63	One-step synthesis of Co-doped 1T-MoS2 nanosheets with efficient and stable HER activity in alkaline solutions. Materials Chemistry and Physics, 2020, 244, 122642.	4.0	51
64	Surface Fluorination Engineering of NiFe Prussian Blue Analogue Derivatives for Highly Efficient Oxygen Evolution Reaction. ACS Applied Materials & Interfaces, 2021, 13, 5142-5152.	8.0	51
65	One-step synthesis of AgBr microcrystals with different morphologies by ILs-assisted hydrothermal method. CrystEngComm, 2011, 13, 1789.	2.6	50
66	Enhancing visible light photocatalytic activity of TiO2 using a colorless molecule (2-methoxyethanol) due to hydrogen bond effect. Applied Catalysis B: Environmental, 2017, 200, 230-236.	20.2	50
67	Ni3B as a highly efficient and selective catalyst for the electrosynthesis of hydrogen peroxide. Applied Catalysis B: Environmental, 2020, 279, 119371.	20.2	48
68	Probing the Mechanism of Plasmon-Enhanced Ammonia Borane Methanolysis on a CuAg Alloy at a Single-Particle Level. ACS Catalysis, 2021, 11, 10814-10823.	11.2	48
69	Fabrication of BiVO4 photoanode consisted of mesoporous nanoparticles with improved bulk charge separation efficiency. Applied Catalysis B: Environmental, 2018, 238, 586-591.	20.2	47
70	Biasâ€Free Solar Water Splitting by Tetragonal Zircon BiVO <sub>4</sub> Nanocrystal Photocathode and Monoclinic Scheelite BiVO <sub>4</sub> Nanoporous Photoanode. Advanced Functional Materials, 2021, 31, 2008656.	14.9	45
71	In-situ growth of Ti3C2@MIL-NH2 composite for highly enhanced photocatalytic H2 evolution. Chemical Engineering Journal, 2021, 411, 128446.	12.7	45
72	Space-confined growth of lead-free halide perovskite Cs3Bi2Br9 in MCM-41 molecular sieve as an efficient photocatalyst for CO2 reduction at the gasâ^'solid condition under visible light. Applied Catalysis B: Environmental, 2022, 310, 121375.	20.2	43

#	Article	IF	CITATIONS
73	Efficient spatial charge separation and transfer in ultrathin g-C <sub>3</sub> N <sub>4</sub> nanosheets modified with Cu <sub>2</sub> MoS <sub>4</sub> as a noble metal-free co-catalyst for superior visible light-driven photocatalytic water splitting. Catalysis Science and Technology, 2018, 8, 3883-3893.	4.1	42
74	Improved photocatalytic CO2 and epoxides cycloaddition via the synergistic effect of Lewis acidity and charge separation over Zn modified UiO-bpydc. Applied Catalysis B: Environmental, 2022, 301, 120793.	20.2	42
75	Plasmon-Mediated Nitrobenzene Hydrogenation with Formate as the Hydrogen Donor Studied at a Single-Particle Level. ACS Catalysis, 2021, 11, 3801-3809.	11.2	41
76	Plasmon-induced dehydrogenation of formic acid on Pd-dotted Ag@Au hexagonal nanoplates and single-particle study. Applied Catalysis B: Environmental, 2020, 277, 119226.	20.2	40
77	Photocatalytic Overall Water Splitting over MILâ€125(Ti) upon CoPi and Pt Coâ€catalyst Deposition. ChemistryOpen, 2017, 6, 701-705.	1.9	39
78	Strain Adjustment Realizes the Photocatalytic Overall Water Splitting on Tetragonal Zircon BiVO <sub>4</sub> . Advanced Science, 2022, 9, e2105299.	11.2	37
79	Electrodeposition of NiFe layered double hydroxide on Ni3S2 nanosheets for efficient electrocatalytic water oxidation. International Journal of Hydrogen Energy, 2020, 45, 8659-8666.	7.1	35
80	Simultaneous SO2/NO removal performance of carbide slag pellets by bagasse templating in a bubbling fluidized bed reactor. Fuel Processing Technology, 2018, 180, 75-86.	7.2	34
81	A water-stable triazine-based metal-organic framework as an efficient adsorbent of Pb(II) ions. Colloids and Surfaces A: Physicochemical and Engineering Aspects, 2019, 560, 315-322.	4.7	34
82	Substrate-dependent ALD of Cux on TiO2 and its performance in photocatalytic CO2 reduction. Chemical Engineering Journal, 2021, 405, 126654.	12.7	34
83	CaO/CaCO3 thermochemical heat storage performance of CaO-based micrometre-sized tubular composite. Energy Conversion and Management, 2020, 222, 113222.	9.2	34
84	Molten-salt assisted synthesis of Cu clusters modified TiO2 with oxygen vacancies for efficient photocatalytic reduction of CO2 to CO. Chemical Engineering Journal, 2022, 445, 136718.	12.7	34
85	Intense Single Red Emission Induced by Nearâ€Infrared Irradiation Using a Narrow Bandgap Oxide BiVO <sub>4</sub> as the Host for Yb <sup>3+</sup> and Tm <sup>3+</sup> lons. Advanced Optical Materials, 2018, 6, 1701331.	7.3	33
86	CO <sub>2</sub> capture by a novel CaO/MgO sorbent fabricated from industrial waste and dolomite under calcium looping conditions. New Journal of Chemistry, 2019, 43, 5116-5125.	2.8	33
87	Density Functional Theory Study on CO <sub>2</sub> Adsorption by Ce-Promoted CaO in the Presence of Steam. Energy & Fuels, 2020, 34, 6197-6208.	5.1	31
88	Boron containing metal–organic framework for highly selective photocatalytic production of H <sub>2</sub> O <sub>2</sub> by promoting two-electron O <sub>2</sub> reduction. Materials Horizons, 2021, 8, 2842-2850.	12.2	31
89	Plasmon-Enhanced Water Activation for Hydrogen Evolution from Ammonia-Borane Studied at a Single-Particle Level. ACS Catalysis, 2022, 12, 3558-3565.	11.2	31
90	Development of Mn/Mg-copromoted carbide slag for efficient CO2 capture under realistic calcium looping conditions. Chemical Engineering Research and Design, 2020, 141, 380-389.	5.6	30

#	Article	IF	CITATIONS
91	Two transition metal phosphonate photocatalysts for H <sub>2</sub> evolution and CO <sub>2</sub> reduction. Chemical Communications, 2018, 54, 7195-7198.	4.1	28
92	ZnO nanorod decorated by Au-Ag alloy with greatly increased activity for photocatalytic ethylene oxidation. Chinese Journal of Catalysis, 2020, 41, 1613-1621.	14.0	28
93	Simultaneous NO/CO2 removal performance of biochar/limestone in calcium looping process. Fuel, 2020, 262, 116428.	6.4	27
94	Simultaneous NO/CO2 removal by Cu-modified biochar/CaO in carbonation step of calcium looping process. Chemical Engineering Journal, 2020, 392, 123659.	12.7	27
95	Ag <sub>2</sub> ZnSnS <sub>4</sub> /Mo-mesh photoelectrode prepared by electroplating for efficient photoelectrochemical hydrogen generation. Journal of Materials Chemistry A, 2019, 7, 1647-1657.	10.3	26
96	Agn+ quantum dots obtained via in situ photodeposition method as photocatalytic CO2 reduction cocatalyst: Borrowing redox conversion between Ag+ and Ag0. Applied Catalysis B: Environmental, 2019, 243, 381-385.	20.2	26
97	Honeycomb Carbon Nanofibers: A Superhydrophilic O <sub>2</sub> â€Entrapping Electrocatalyst Enables Ultrahigh Mass Activity for the Twoâ€Electron Oxygen Reduction Reaction. Angewandte Chemie, 2021, 133, 10677-10681.	2.0	26
98	Enhanced selectivity and activity for electrocatalytic reduction of CO <sub>2</sub> to CO on an	10.3	25
99	Boosting H <sub>2</sub> Production from a BiVO <sub>4</sub> Photoelectrochemical Biomass Fuel Cell by the Construction of a Bridge for Charge and Energy Transfer. Advanced Materials, 2022, 34, e2201594.	21.0	24
100	Tailoring the composition and structure of Ni3S2 by introduction of Co towards high efficiency energy storage device. Chemical Engineering Journal, 2021, 403, 126285.	12.7	23
101	Nitrogen vacancy enhanced photocatalytic selective oxidation of benzyl alcohol in g-C3N4. International Journal of Hydrogen Energy, 2021, 46, 37782-37791.	7.1	23
102	TiN nanosheet arrays on Ti foils for high-performance supercapacitance. RSC Advances, 2018, 8, 12841-12847.	3.6	22
103	ZnO nanorods modified with noble metal-free Co <sub>3</sub> O <sub>4</sub> nanoparticles as a photocatalyst for efficient ethylene degradation under light irradiation. Catalysis Science and Technology, 2019, 9, 6191-6198.	4.1	22
104	Oxygen vacancy enhancing CO2 electrochemical reduction to CO on Ce-doped ZnO catalysts. Surfaces and Interfaces, 2021, 23, 100923.	3.0	22
105	Targeted Regulation of the Electronic States of Nickel Toward the Efficient Electrosynthesis of Benzonitrile and Hydrogen Production. ACS Applied Materials & Interfaces, 2021, 13, 56140-56150.	8.0	21
106	Atomically dispersed cobalt-based species anchored on polythiophene as an efficient electrocatalyst for oxygen evolution reaction. Applied Surface Science, 2021, 545, 148943.	6.1	19
107	Photo-induced photo-thermal synergy effect leading to efficient CO2 cycloaddition with epoxide over a Fe-based metal organic framework. Journal of Colloid and Interface Science, 2022, 625, 33-40.	9.4	19
108	Enhanced electrocatalytic HER performance of non-noble metal nickel by introduction of divanadium trioxide. Electrochimica Acta, 2019, 320, 134535.	5.2	18

#	Article	IF	CITATIONS
109	Monomolecular VB <sub>2</sub> -doped MOFs for photocatalytic oxidation with enhanced stability, recyclability and selectivity. Journal of Materials Chemistry A, 2019, 7, 26934-26943.	10.3	18
110	Molybdenum Nitride Electrocatalysts for Hydrogen Evolution More Efficient than Platinum/Carbon: Mo <sub>2</sub> N/CeO <sub>2</sub> @Nickel Foam. ACS Applied Materials & Interfaces, 2020, 12, 29153-29161.	8.0	18
111	Understanding the enhancement of CaO on water gas shift reaction for H2 production by density functional theory. Fuel, 2021, 303, 121257.	6.4	18
112	Enhanced photocatalytic hydrogen evolution ofÂCdWO4 through polar organic molecule modification. International Journal of Hydrogen Energy, 2019, 44, 4754-4763.	7.1	17
113	Photococatalytic anticancer performance of naked Ag/AgCl nanoparticles. Chemical Engineering Journal, 2022, 428, 131265.	12.7	17
114	In Situ Monitoring Charge Transfer on Topotactic Epitaxial Heterointerface for Tetracycline Degradation at the Single-Particle Level. ACS Catalysis, 2022, 12, 9114-9124.	11.2	17
115	CdS–MoS <sub>2</sub> heterostructures on Mo substrates via in situ sulfurization for efficient photoelectrochemical hydrogen generation. RSC Advances, 2017, 7, 44626-44631.	3.6	16
116	Energy storage and attrition performance of limestone under fluidization during CaO/CaCO3 cycles. Energy, 2020, 207, 118291.	8.8	16
117	CaO/Ca(OH)2 heat storage performance of hollow nanostructured CaO-based material from Ca-looping cycles for CO2 capture. Fuel Processing Technology, 2021, 217, 106834.	7.2	16
118	Synergistic effect between boron containing metal-organic frameworks and light leading to enhanced CO2 cycloaddition with epoxides. Chemical Engineering Journal, 2022, 437, 135363.	12.7	16
119	Formation mechanism of rectangular-ambulatory-plane TiO <sub>2</sub> plates: an insight into the role of hydrofluoric acid. Chemical Communications, 2018, 54, 7191-7194.	4.1	15
120	Enhanced singlet oxygen production over a photocatalytic stable metal organic framework composed of porphyrin and Ag. Journal of Colloid and Interface Science, 2021, 602, 300-306.	9.4	15
121	Promoting Electrocatalytic Reduction of CO <sub>2</sub> to C <sub>2</sub> H <sub>4</sub> Production by Inhibiting C <sub>2</sub> H <sub>5</sub> OH Desorption from Cu <sub>2</sub> O/C Composite. Small, 2022, 18, e2105212.	10.0	15
122	BiVO <sub>4</sub> quadrangular nanoprisms with highly exposed {101} facets for selective photocatalytic oxidation of benzylamine. Journal of Materials Chemistry A, 2022, 10, 19699-19709.	10.3	15
123	Effects of Ag Incorporation on the Band Structures and Conductivity Types of (Cu <sub>1â€<i>x</i></sub> Ag <sub><i>x</i></sub> ) <sub>2</sub> ZnSnS <sub>4</sub> Solid Solutions. ChemPhotoChem, 2018, 2, 811-817.	3.0	14
124	Enhanced photocatalytic activity towards H2 evolution over NiO via phosphonic acid surface modification with different functional groups. International Journal of Hydrogen Energy, 2019, 44, 16575-16581.	7.1	14
125	Post-synthetic platinum complex modification of a triazine based metal organic frameworks for enhanced photocatalytic H2 evolution. Journal of Solid State Chemistry, 2019, 271, 260-265.	2.9	14
126	In situ integration of Fe3N@Co4N@CoFe alloy nanoparticles as efficient and stable electrocatalyst for overall water splitting. Electrochimica Acta, 2021, 395, 139218.	5.2	14

#	Article	IF	CITATIONS
127	CaO/H <sub>2</sub> 0 Thermochemical Heat Storage Capacity of a CaO/CeO <sub>2</sub> Composite from CO <sub>2</sub> Capture Cycles. Industrial & Engineering Chemistry Research, 2020, 59, 16741-16750.	3.7	13
128	The effect of Cu on NO reduction by char with density functional theory in carbonation stage of calcium looping. Fuel, 2021, 283, 119332.	6.4	13
129	Efficient Photocatalytic Hydrogen Generation from Water over CdS Nanoparticles Confined Within an Alumina Matrix. ChemPhotoChem, 2017, 1, 518-523.	3.0	12
130	αâ€Fe <sub>2</sub> O <sub>3</sub> Film with Highly Photoactivity for Nonâ€enzymatic Photoelectrochemical Detection of Glucose. Electroanalysis, 2019, 31, 1809-1814.	2.9	12
131	Coupled CO <sub>2</sub> capture and thermochemical heat storage of CaO derived from calcium acetate. , 2020, 10, 1027-1038.		11
132	Synthesis of novel cubic Ni2Mo3N and its electronic structure regulation by vanadium doping towards high-efficient HER electrocatalyst. Electrochimica Acta, 2020, 337, 135689.	5.2	11
133	Host dependent electrocatalytic hydrogen evolution of Ni/TiO2 composites. Journal of Materials Chemistry A, 2021, 9, 6325-6334.	10.3	10
134	Strain-assisted in-situ formed oxygen defective WO3 film for photothermal-synergistic reverse water gas shift reaction and single-particle study. Chemical Engineering Journal, 2022, 433, 134199.	12.7	10
135	Borate-modulated amorphous NiFeB nanocatalysts as highly active and stable electrocatalysts for oxygen evolution reaction. Journal of Alloys and Compounds, 2022, 903, 163741.	5.5	10
136	Simultaneous CO <sub>2</sub> capture and heat storage by a Ca/Mg-based composite in coupling calcium looping and CaO/Ca(OH) <sub>2</sub> cycles using air as a heat transfer fluid. Reaction Chemistry and Engineering, 2021, 6, 100-111.	3.7	9
137	Photothermal synergy for efficient dry reforming of CH <sub>4</sub> by an Ag/AgBr/CsPbBr <sub>3</sub> composite. Catalysis Science and Technology, 2022, 12, 1628-1636.	4.1	9
138	Photostable Ag(I)-Based Metal–Organic Framework: Synthesis, Structure, and Photocatalytic Selective Oxidation Properties. Inorganic Chemistry, 2020, 59, 16127-16131.	4.0	8
139	Tuning the Conduction Band Potential of Biâ€based Semiconductors Using a Combination of Organic Ligands. ChemSusChem, 2021, 14, 892-897.	6.8	7
140	Ag/AgCl as an efficient plasmonic photocatalyst for greenhouse gaseous methane oxidation. Journal of Environmental Chemical Engineering, 2021, 9, 106435.	6.7	7
141	In situ extract nucleate sites for the growth of free-standing carbon nitride films on various substrates. Catalysis Today, 2020, 340, 92-96.	4.4	6
142	A Bismuth-Based Metal–Organic Framework for Visible-Light-Driven Photocatalytic Decolorization of Dyes and Oxidation of Phenylboronic Acids. Inorganic Chemistry, 2022, 61, 11110-11117.	4.0	6
143	Design and synthesis of BiVO4@CuOx as a photo assisted Fenton-like catalyst for efficient degradation of tetracycline. Surfaces and Interfaces, 2021, 26, 101380.	3.0	5
144	Boosting hot electrons transfer via laser-induced atomic redistribution for plasmon-enhanced nitroreduction and single-particle study. Journal of Catalysis, 2022, 407, 115-125.	6.2	4

#	Article	IF	CITATIONS
145	Photoelectrochemical Oxidation of Amines to Imines and Production of Hydrogen through Mo-Doped BiVO <sub>4</sub> Photoanode. ACS Omega, 2022, 7, 12816-12824.	3.5	4
146	In Situ Preparation of CsPbBr <sub>3</sub> @CsPb <sub>2</sub> Br <sub>5</sub> Composite Assisted with Water as a Highly Efficient and Stable Catalyst for Photothermal CO <sub>2</sub> Hydrogenation. Chemistry - A European Journal, 2022, 28, .	3.3	4
147	SO2 removal performances of Al- and Mg-modified carbide slags from CO2 capture cycles at calcium looping conditions. Journal of Thermal Analysis and Calorimetry, 2021, 144, 1187-1197.	3.6	3
148	NiCoP–CeO <sub>2</sub> composites for efficient electrochemical oxygen evolution. RSC Advances, 2022, 12, 13639-13644.	3.6	2
149	Growth of bulk BiOBr single crystals for the characterization of intrinsic semi-conductive properties and application in ultraviolet photodetectors. Journal of Materials Chemistry C, 2022, 10, 10330-10337.	5.5	2
150	BiVO4 Ceramic Photoanode with Enhanced Photoelectrochemical Stability. Nanomaterials, 2021, 11, 2404.	4.1	1
151	Enhancing Electrocatalytic N2 Conversion to NH3 by MnO2 Ultralong Nanowires with Oxygen Vacancies. Journal of Photocatalysis, 2021, 2, 140-146.	0.4	0
152	Synthesis of photocatalytic hybrid nanostructures. , 2022, , .		0
153	In situ observation of photo-induced shortening of single Au nanorod for plasmon-enhanced formic acid dehydrogenation. , 2022, , 100014.		0